



Electrocaloric effect and pyroelectric energy harvesting in diffuse ferroelectric $\text{Ba}(\text{Ti}_{1-x}\text{Ce}_x)\text{O}_3$ ceramics

Y. Zhao¹ · X. Q. Liu¹ · S. Y. Wu¹ · X. M. Chen¹

Received: 11 July 2018 / Accepted: 26 August 2019 / Published online: 31 August 2019
© Springer Science+Business Media, LLC, part of Springer Nature 2019

Abstract

In the present work $\text{Ba}(\text{Ti}_{1-x}\text{Ce}_x)\text{O}_3$ ceramics are prepared through a standard solid-state sintering process. Crystal structures, dielectric properties, ferroelectric properties and electrocaloric effects are exactly studied. Ce^{4+} ions cannot entirely enter the position of Ti^{4+} , so some impure phases are generated. The diffusivity of phase transition is strengthened by substituting Ti^{4+} with Ce^{4+} cations. The maximal pyroelectric coefficient decreases, and the extent of corresponding temperature deviating from the dielectric peak temperature to higher temperature increases with increasing the content of cerium cations. The adiabatic temperature change and isothermal entropy change display the same tendency as that of the pyroelectric coefficient. The $\text{Ba}(\text{Ti}_{0.9}\text{Ce}_{0.1})\text{O}_3$ ceramic shows the largest adiabatic temperature change of 0.41 K and the largest isothermal entropy change of 0.45 J/(kg·K) among the ceramics. Accordingly, the adiabatic temperature change responsivity is 0.090×10^{-6} K·m/V, and the isothermal entropy change responsivity is 0.100×10^{-6} J·m/(kg·K·V). For individual composition, the absolute value of pyroelectric coefficient decreases with increasing the magnitude of applied electric field, and the temperature of maximal pyroelectric coefficient deviates from the dielectric peak temperature shifts to higher temperature. $\text{Ba}(\text{Ti}_{0.9}\text{Ce}_{0.1})\text{O}_3$ ceramics show the largest pyroelectric energy density of 0.14 J/cm³ among all compositions.

Keywords Electrocaloric effect · Pyroelectric energy harvesting · Diffuse ferroelectric

1 Introduction

Traditional vapor-compression technology has been used over 100 years in refrigeration field, while it comes to the end of improving energy-cost efficiency. Solid state refrigeration technology has been proposed as promising representative due to high efficiency, environment friendly, low cost and so on. Electrocaloric effect is firstly observed in Rochelle Salt in 1930 [1], it is neglected for a long time until Mischenko et al. have a giant electrocaloric effect of about 12 K in $\text{PbZr}_{0.95}\text{Ti}_{0.05}\text{O}_3$ thin film in 2006 [2], then numerous papers about electrocaloric effect are published. Electrocaloric effect can be simply thought as adiabatic temperature change or isothermal entropy change upon apply or removal of electric field of materials [3]. In the view of saving energy,

pyroelectric effect as the converse effect of electrocaloric effect has been investigated [4–6]. Pyroelectric effect exists intrinsically in polar materials, the surfaces of the materials gain charge due to spontaneous polarization, further heat exchange with the surrounding leads to charge change. It is to say pyroelectric effect can be utilized to transform waste heat into electric energy [7], while waste heat consumes a large content of energy cost.

BaTiO_3 is typical perovskite structure material, either Ba^{2+} or Ti^{4+} can be substituted by iso-valent ions or hetero-valent ions. Since the structure of BaTiO_3 is simple, different ions substituted BaTiO_3 materials have been extensively studied [8–21], and the dielectric permittivity, ferroelectric property and microstructure are influenced by the substitution. Electrocaloric effect seemed to be linked to the dielectric properties, ferroelectric properties and microstructure, but the characteristics of electrocaloric effect are originally from the substitution of other ions. Three phase transitions exist in BaTiO_3 , while they will merge into one point at a certain substitution quantity as the substitution quantity of other ions increases. The merged point is called invariant critical point (ICP) [11, 14], Qian et al. have reported the adiabatic temperature change of 4.5 K at

✉ X. Q. Liu
xqliu@zju.edu.cn

¹ Laboratory of Dielectric Materials, School of Materials Science and Engineering, Zhejiang University, No. 38 Zheda Road, Hangzhou 310027, China

invariant critical point in Zr^{4+} substituted $BaTiO_3$ materials [11]. Electrocaloric effect is a promising candidate in industry cooling, while some problems should be conquered. The materials should achieve considerable adiabatic temperature change and isothermal entropy change at the same time, which can ensure the exchange heat capacity large enough. Considering the household voltage is limited, the driving efficiency of electric field for electrocaloric effect is focused, the electrocaloric effect responsivities were recently proposed [22–27]. Electrocaloric effect responsivities are introduced as $\Delta T/\Delta E$ and $\Delta S/\Delta E$ respectively.

Recently, Srikanth [28] reported electrocaloric effect in $Ba(Ti_{1-x}Ce_x)O_3$ ceramics, adiabatic temperature change responsivity of 0.35×10^{-6} K·m/V was achieved, and Zeng [29] achieved adiabatic temperature change 0.61 K at 30 kV/cm for $Ba(Ti_{0.9}Ce_{0.1})O_3$ ceramics. Yet the effect of diffuse behaviour on electrocaloric effect was not discussed yet. In present work $Ba(Ti_{1-x}Ce_x)O_3$ ceramics were prepared by a standard solid-state sintering method, and the linkage between different properties are discussed, and the influence of diffuse ferroelectricity on electrocaloric effect is exactly discussed.

2 Experimental procedure

$Ba(Ti_{1-x}Ce_x)O_3$ ceramics with compositions of $x = 0.10, 0.15$ and 0.20 were prepared by a standard solid-state reaction method. Powders of raw materials with high purity, i.e., $BaCO_3$ (99.99%), TiO_2 (99.99%) and CeO_2 (99.99%) were weighed in stoichiometric ratio, ball mixed in distilled water and zirconia media for 24 h and then dried. The mixtures were calcined at 1150 °C for 3 h in air. After regrinding, calcined powders were added 8 wt% PVA, then the mixtures were compacted at 2 MPa for 1 min into pellets. The pellets were sintered at 1525 °C for 6 h in air.

The crystal structures were identified using powder X-ray diffraction (XRD, RIGAKU D/max 2550/PC, Rigaku Co., Tokyo, Japan) at room temperature. The data for Rietveld refinement were collected at the 2θ range of 8–130° with the step of 0.02°. The Rietveld refinement was carried out using the Fullprof program [30]. The densities of samples were measured by Archimede method. Temperature dependence of dielectric permittivity was evaluated using a broad-band dielectric spectrometer (Turnkey Concept 50, Novocontrol Technologies GmbH & Co. KG, Hundsangen, Germany) with Au pasted. P - E hysteresis loops were measured at 10 Hz every 5 °C using a Precision Analyzer (Precision Premier II, Radiant Technologies, Albuquerque, NM, USA) combined with Sigma temperature controller. Heat capacity was measured using a differential scanning calorimeter (DSC, Netzsch DSC204 F1, Selb, Germany) apparatus.

3 Results and discussions

Room-temperature XRD patterns of $Ba(Ti_{1-x}Ce_x)O_3$ ceramic powders are shown in Fig. 1. To identify the crystal structures of the ceramics, the space groups of $Pm\bar{3}m$, $P4mm$ or mixture are tested. According to the Rietveld refinement results, the $P4mm$ phase is adopted, and the results are shown in Table 1. In addition to the major phase, three minor phases, CeO_2 , Ba_2TiO_4 and TiO_2 , exist in the ceramics, implying that Ce^{4+} cannot entirely enter the position of Ti^{4+} . The actual Ce/Ti ratio should be different to the nominal one since some CeO_2 and TiO_2 impure phases are existed in the ceramics, and the ratio is critical to the Curie temperature. Indeed, the ratio refined from the structural analysis is different as shown in Table 1. The real ratio is lower than that of nominal one, indicating the real Curie temperature should be higher than the expected one. The cell parameters, a , c and cell volume monotonously increase with the content of Ce^{4+} cations because of the larger ionic radius (0.87 vs. 0.605 Å). The c/a parameters almost decrease with increasing the content of Ce^{4+} cations, indicating the decreased ferroelectric properties, and the Curie temperature should decrease successively. Figure 2 shows the SEM micrographs of $Ba(Ti_{1-x}Ce_x)O_3$ ceramics ($x = 0.1, 0.15$ and 0.2), the microstructure is considerably dense, which is in agreement with the high relative densities of all samples (>97%).

Figure 3 shows the temperature dependence of relative permittivity of $Ba(Ti_{1-x}Ce_x)O_3$ ceramics at various frequencies. The temperature dependence of relative permittivity shows a broad maximum with frequency dispersion, which is known as diffuse phase transition. According to results reported by Han [21], the pure $BaTiO_3$ ceramics show a sharp peak, while peaks of doping compositions show broaden shapes. The broaden maximum of $Ba(Ti_{0.9}Ce_{0.1})O_3$ ceramics represents a diffuse phase transition. In the diffuse ferroelectric, addition to the structural phase transition to ferroelectric state with macroscopic domains, the nano-sized polarization regions (PNRs) appear embedded in the paraelectric matrix at the temperature above the permittivity peak temperature [31–34]. In accordance with the previous work [34], the $Ba(Ti_{1-x}Ce_x)O_3$ ceramic shows the same phenomenon, as the content of Ce^{4+} increases the dielectric peak becomes broader, implying that the Ce^{4+} doping strengthens the diffusivity of the phase transition. Figure 3 also shows the temperature dependence of dielectric loss of $Ba(Ti_{1-x}Ce_x)O_3$ at various frequencies. A frequency-dispersed peak correspond to the permittivity peak appears. The dielectric loss in the measured temperature period varies lower than 0.1. As the substitution quantity of Ce^{4+} increases, the temperature of permittivity peak decreases monotonically. The temperature of permittivity peak of $Ba(Ti_{1-x}Ce_x)O_3$ ceramics are 378 K, 358 K and 318 K for $x = 0.1, 0.15$ and 0.2 , respectively. Figure 4 shows the

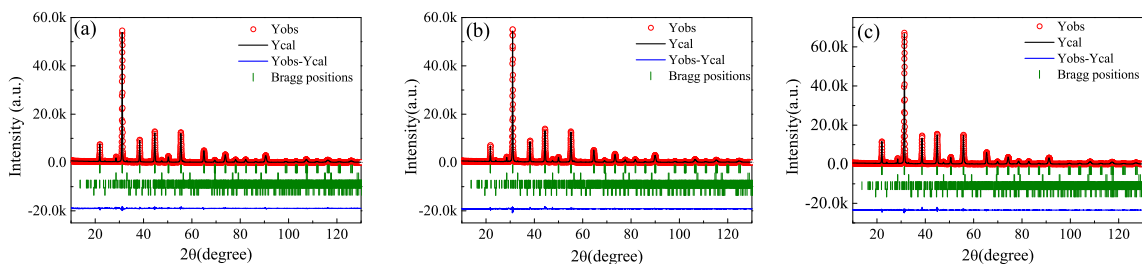


Fig. 1 XRD patterns and Rietveld refinement results of $\text{Ba}(\text{Ti}_{1-x}\text{Ce}_x)\text{O}_3$ ceramics: (a) $x = 0.10$, (b) $x = 0.15$ and (c) $x = 0.20$. The Bragg positions for major, CeO_2 , Ba_2TiO_4 and TiO_2 phases are listed from the top to bottom, respectively

modified Curie-Weiss fitting of $\text{Ba}(\text{Ti}_{1-x}\text{Ce}_x)\text{O}_3$ ceramic, the diffuseness exponents can be derived from the relation between logarithm of reciprocal relative dielectric permittivity and logarithm of temperature [35, 36]. The diffuseness exponents (γ) are 1.71, 1.74 and 1.90 for $x = 0.1$, 0.15 and 0.2, respectively. As in Fig. 3, the permittivity peaks get broader and the permittivity values get lower with more Ce^{4+} substituted, it can be illustrated by the diffuseness exponents derived from the modified Curie-Weiss fitting.

Electrocaloric effect is defined as adiabatic temperature change and isothermal entropy change during the application or removal of electric field. Considering the practical application of ECE, both large isothermal entropy change and large adiabatic temperature change can ensure large enough refrigeration capacity. In the present work, the indirect method is used to achieve the ECE. Figure 5(a) shows the P - E hysteresis loops of $\text{Ba}(\text{Ti}_{0.9}\text{Ce}_{0.1})\text{O}_3$ ceramic measured under 45 kV/cm at 10 Hz of several temperatures. The frequency of 10 Hz ensures dipoles can rotate sufficiently under the electric field, and the interval

of 5 K ensures enough data of polarizations for polynomial fitting. From Fig. 5(a) one can see the hysteresis loops still exist even the temperature is above the dielectric peak temperature, as the temperature increases, the hysteresis loops become slimmer but different from the linear shape of paraelectric state. Around 408 K the values of maximal polarization change faster than other temperatures, which may be due to the sharply increasing number of PNRs at around 408 K. Figure 5(b) shows the evolution between polarization and temperature for all compositions measured under 45 kV/cm. Pyroelectric coefficients can be derived from the P - T fourth polynomial equation. Figure 5(c) shows the pyroelectric coefficients at various temperatures for all compositions. The temperature period covers from the dielectric peak temperature to 70 K above that temperature. According to the calculation equation of ECE, pyroelectric coefficient is dominant factor of ECE. From Fig. 5(c) one can roughly predict that $\text{Ba}(\text{Ti}_{0.9}\text{Ce}_{0.1})\text{O}_3$ sample may have largest ECE among all compositions. And the largest pyroelectric

Table 1 Rietveld results of XRD patterns of major phase of $\text{Ba}(\text{Ti}_{1-x}\text{Ce}_x)\text{O}_3$ ceramics at room temperature^{a)}

x	0.10	0.15	0.20
a (Å)	4.03284(11)	4.05558(10)	4.07706(13)
c (Å)	4.04661(16)	4.06721(16)	4.08665(22)
c/a	1.0034	1.0029	1.0024
Volume (Å ³)	65.813(4)	66.896(4)	67.930(5)
Ba B_{iso} (Å ²)	1.121(15)	0.847(14)	1.024(17)
Ti/Ce z	0.4967(49)	0.4971(62)	0.5017(28)
Ti B_{iso} (Å ²)	1.215(35)	1.093(32)	0.996(30)
O1 z	0.0252(88)	0.011(21)	0.0339(84)
O2 z	0.5367(55)	0.5314(75)	0.5494(56)
Ce/Ti ratio	0.050(5)/0.950(5)	0.136(6)/0.864(6)	0.168(5)/0.832(5)
CeO_2 (wt%)	2.25(4)	1.91(4)	2.14(4)
Ba_2TiO_4 (wt%)	1.24(6)	1.22(6)	1.61(6)
TiO_2 (wt%)	1.36(5)	1.05(5)	1.49(6)
R_p (%)	5.98	5.47	5.88
R_{wp} (%)	9.06	8.14	8.61
χ^2	5.96	3.87	4.56

^{a)} Space group: $P4mm$, Ba at $1a$ (0, 0, 0), Ti/Ce at $1b$ (0.5, 0.5, z), O1 at $1b$ (0.5, 0.5, z), and O2 at $2c$ (0.5, 0, z)

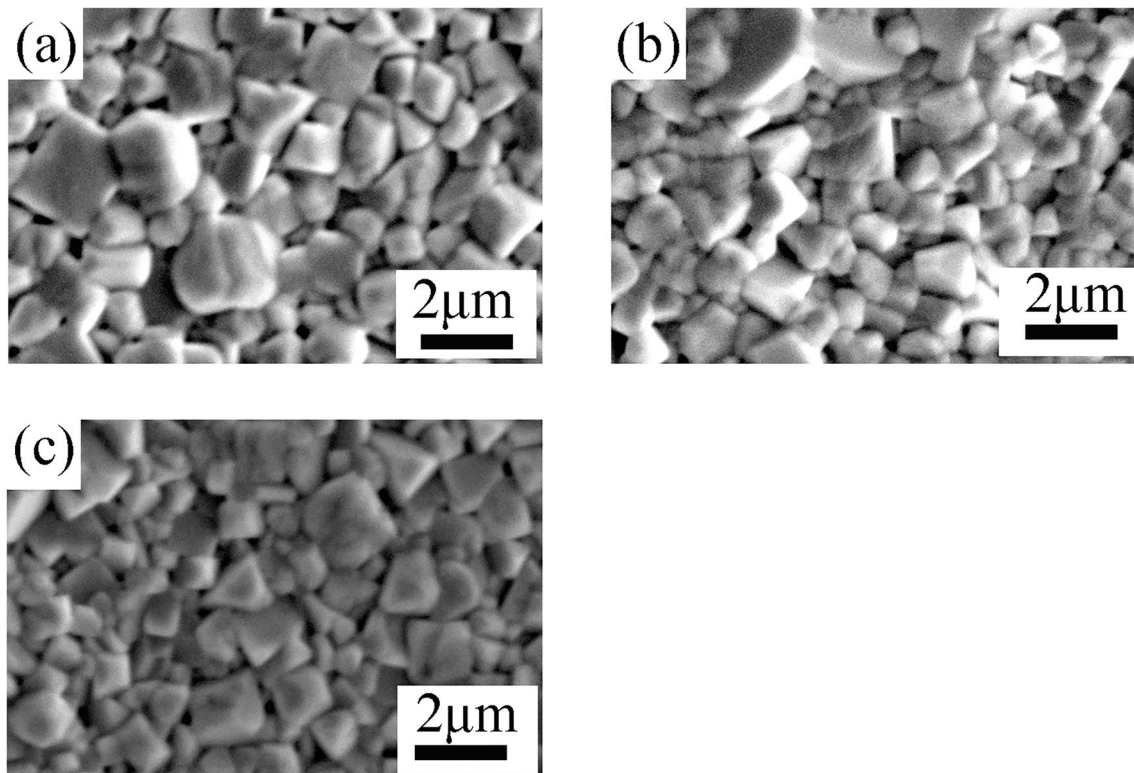


Fig. 2 SEM micrographs of $\text{Ba}(\text{Ti}_{1-x}\text{Ce}_x)\text{O}_3$ ceramics: (a) $x = 0.1$, (b) $x = 0.15$ and (c) $x = 0.2$

coefficient of $\text{Ba}(\text{Ti}_{0.9}\text{Ce}_{0.1})\text{O}_3$ sample locates at 408 K, which is in agreement with the inflection point in Fig. 5(a). The pyroelectric coefficient decreases with increasing the content of Ce^{4+} cations. The maximal pyroelectric coefficient locates several kelvins above the dielectric peak temperature, implying the maximal ECE may locate at the temperature above the dielectric peak temperature. The extent of temperature corresponding to the maximal pyroelectric coefficient deviates from the dielectric peak temperature to higher temperature increases with increasing the content of Ce^{4+} cations (see Table 2). The variation of pyroelectric coefficient with Ce^{4+} content may be linked to the extent of diffuseness of phase transition, and it will lead to the variation of electrocaloric properties of the $\text{Ba}(\text{Ti}_{1-x}\text{Ce}_x)\text{O}_3$ ceramics.

Figure 6 shows the ECE values and ECE responsivities of all compositions under the external electric field of 45 kV/cm. Figure 6(a) shows the temperature dependence of adiabatic temperature change, and the curves are smooth indicating comparably stable adiabatic temperature change in a broad temperature period since all compositions show diffuse phase transition. $\text{Ba}(\text{Ti}_{0.9}\text{Ce}_{0.1})\text{O}_3$ ceramic achieves the largest adiabatic temperature change 0.41 K among all compositions, and its permittivity is also largest among all compositions. $\text{Ba}(\text{Ti}_{0.8}\text{Ce}_{0.2})\text{O}_3$ ceramic shows the largest difference 50 K between

temperature corresponding to permittivity peak and that of maximal electrocaloric effect (see Table 2). As the substitution quantity of Ce^{4+} increases, the extent of diffuseness of phase transition strengthens. The largest adiabatic temperature change locates 5 K above the temperature corresponding to maximal pyroelectric coefficient, which is due to the multiplying parts. Figure 6(c) shows the temperature dependence of isothermal entropy change, and the largest isothermal entropy change just locates at the same temperature as pyroelectric coefficient. $\text{Ba}(\text{Ti}_{0.9}\text{Ce}_{0.1})\text{O}_3$ ceramic achieves the largest isothermal entropy change 0.45 J/(kg·K) among all compositions, $\text{Ba}(\text{Ti}_{0.8}\text{Ce}_{0.2})\text{O}_3$ ceramic shows the largest difference 45 K between temperature corresponding to permittivity peak and that of maximal isothermal entropy change. In normal ferroelectrics, the largest ECE locates near the phase transition where the overall material goes through structural change. But in diffuse ferroelectrics, the PNRs begin to appear and embed in the paraelectric matrix at temperature above the dielectric peak temperature. It can be simply understood that the number of PNRs varies more sharply in $\text{Ba}(\text{Ti}_{0.9}\text{Ce}_{0.1})\text{O}_3$ ceramic than the other two compositions, while the polarization quantity of individual PNR is assumed as the same.

Electric field is the driving source of ECEs, parameters describing the efficiency electric field driving ECEs

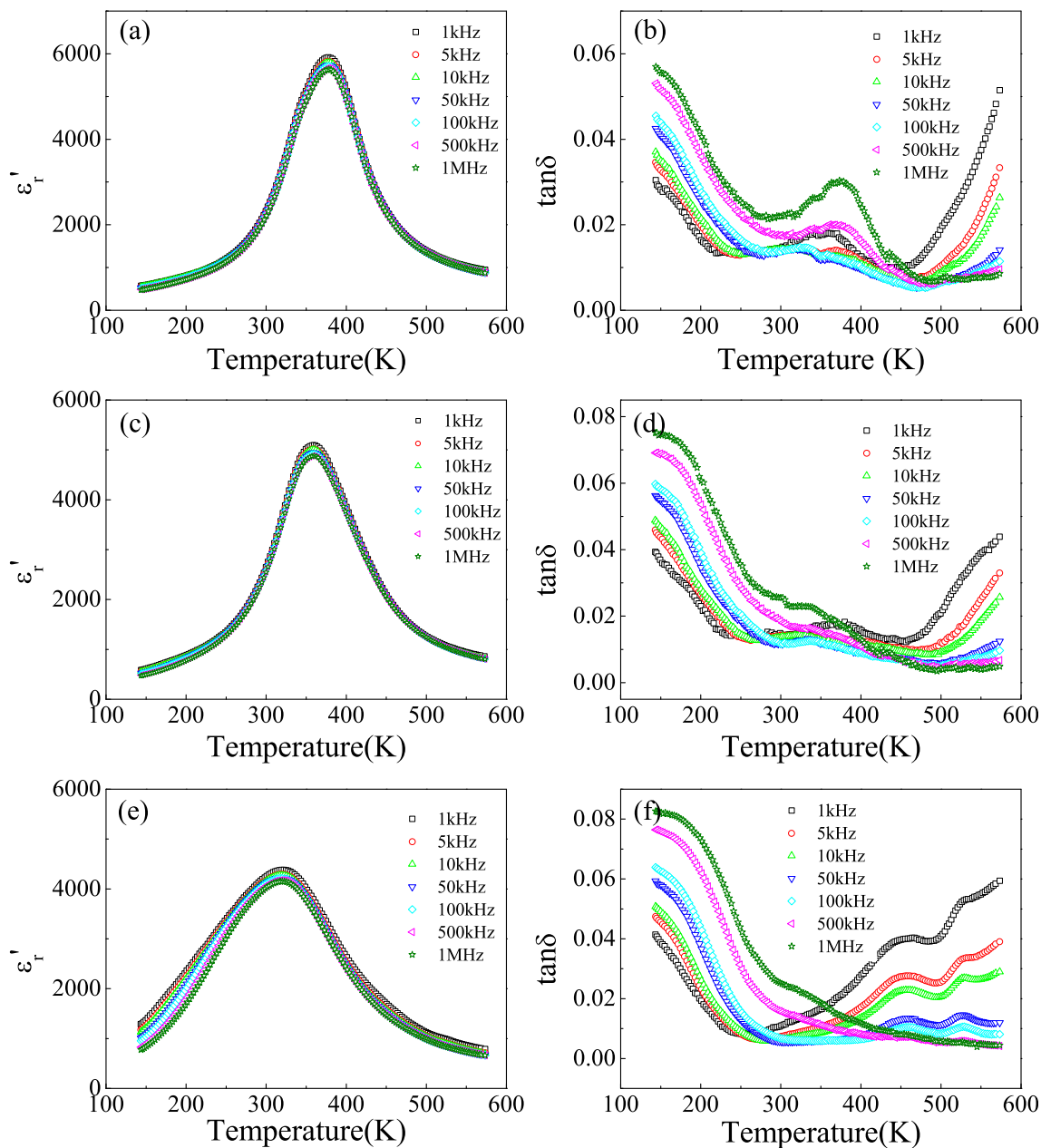


Fig. 3 Temperature dependences of the relative dielectric permittivity of (a) $\text{Ba}(\text{Ti}_{0.9}\text{Ce}_{0.1})\text{O}_3$, (c) $\text{Ba}(\text{Ti}_{0.85}\text{Ce}_{0.15})\text{O}_3$, and (e) $\text{Ba}(\text{Ti}_{0.8}\text{Ce}_{0.2})\text{O}_3$ ceramic measured at various frequencies, respectively. Temperature

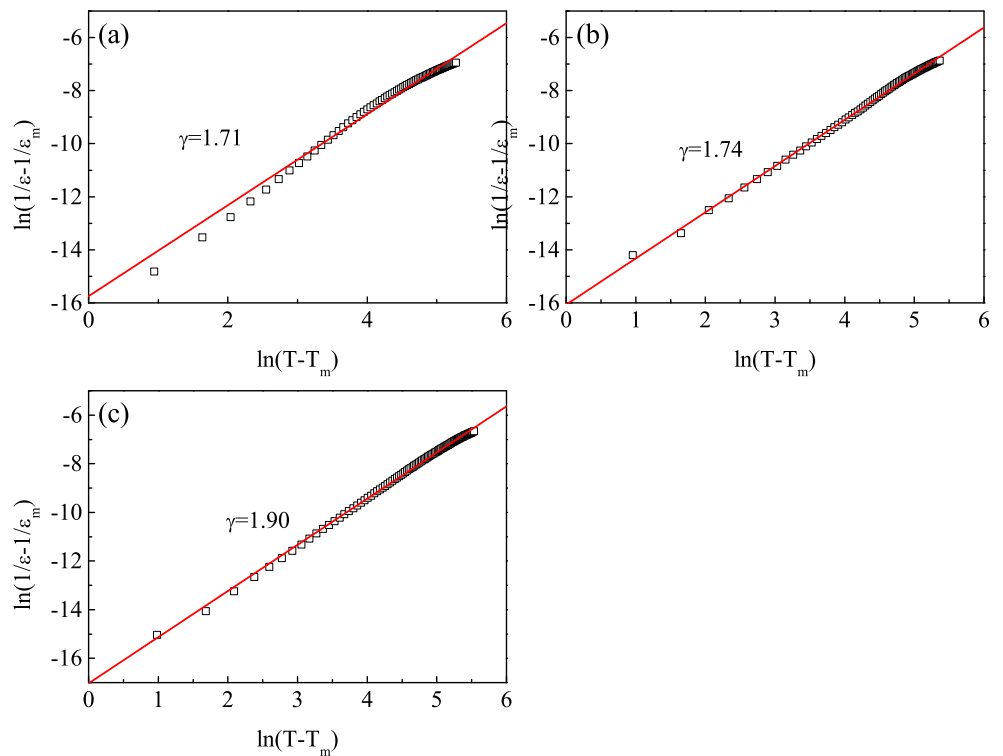
dependences of the dielectric losses of (b) $\text{Ba}(\text{Ti}_{0.9}\text{Ce}_{0.1})\text{O}_3$, (d) $\text{Ba}(\text{Ti}_{0.85}\text{Ce}_{0.15})\text{O}_3$, and (f) $\text{Ba}(\text{Ti}_{0.8}\text{Ce}_{0.2})\text{O}_3$ ceramic measured at various frequencies, respectively

are needed, so electrocaloric temperature change responsivity $\Delta T/\Delta E$ and electrocaloric entropy change responsivity $\Delta S/\Delta E$ are shown in Fig. 6(b) and (d). $\text{Ba}(\text{Ti}_{0.9}\text{Ce}_{0.1})\text{O}_3$ ceramic achieves the largest electrocaloric temperature change responsivity $0.090 \times 10^{-6} \text{ K}\cdot\text{m}/\text{V}$ and largest electrocaloric entropy change responsivity $0.100 \times 10^{-6} \text{ J}\cdot\text{m}/(\text{kg}\cdot\text{K}\cdot\text{V})$ among all compositions. Although the electrocaloric effects in this work are not large compared with those published data [7–18], it can be observed the electrocaloric effects keep moderate values over a broad temperature. T_{span} is

introduced to evaluate the ability materials maintain comparable adiabatic temperature change with the maximal value defined as temperature range over which ΔT maintains $0.9 \times \Delta T_{\text{max}}$. T_{span} values are larger than 25 K for all compositions, indicating the ceramics can keep moderate values over a relative broad temperature range.

To further investigate the ECE of $\text{Ba}(\text{Ti}_{1-x}\text{Ce}_x)\text{O}_3$ ceramics, $\text{Ba}(\text{Ti}_{0.9}\text{Ce}_{0.1})\text{O}_3$ ceramic is chosen to investigate the influence of magnitude of electric field on ECE. Figure 7 lists a series of parameters measured under different electric fields. Figure 7(a) shows the

Fig. 4 Modified Curie-Weiss fitting results of (a) Ba(Ti_{0.9}Ce_{0.1})O₃, (b) Ba(Ti_{0.85}Ce_{0.15})O₃, and (c) Ba(Ti_{0.8}Ce_{0.2})O₃ ceramic at the frequency of 1 MHz, respectively



temperature dependence of pyroelectric coefficient derived from the evolution between polarization and temperature, the maximal pyroelectric coefficient moves to higher temperature and the quantity of maximal pyroelectric coefficient decreases as the magnitude of electric field increases. The maximal pyroelectric coefficient of $-6.25 \times 10^{-4} \text{ C}/(\text{m}^2 \cdot \text{K})$ locates at 403 K under a field of 20 kV/cm, while the coefficient of $-5.65 \times 10^{-4} \text{ C}/(\text{m}^2 \cdot \text{K})$ locates at 408 K under a field of 45 kV/cm. Electrocaloric effect can be understood as the phenomenon that the temperature or entropy of whole material changes due to change of the number of polarized states, which is caused by external electric field in nature. Figure 7(b) and (d) show the temperature

dependence of adiabatic temperature change and isothermal entropy change measured under different magnitudes of electric field, respectively. Figure 7(c) and (e) show the temperature dependence of adiabatic temperature change responsivity and isothermal entropy change responsivity measured under different magnitudes of electric field respectively. The corresponding responsivities show the same changing tendency as the pyroelectric coefficient. The largest adiabatic temperature change responsivity of $0.099 \times 10^{-6} \text{ K} \cdot \text{m}/\text{V}$ among all magnitudes of electric field is achieved at the field of 20 kV/cm. For individual magnitude of electric field, the maximal adiabatic temperature change locates 5 K above the temperature corresponding to maximal

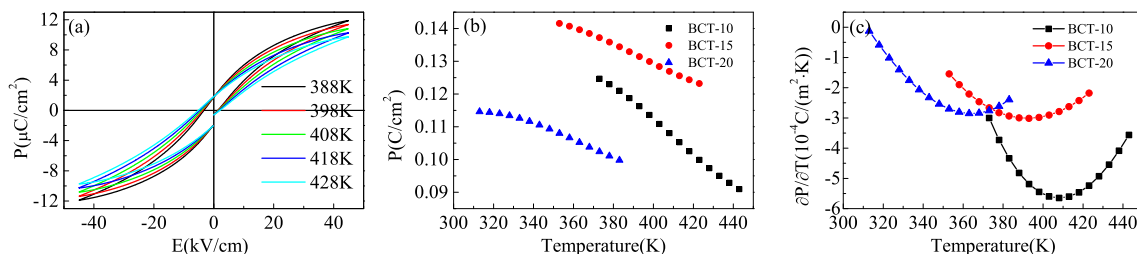


Fig. 5 (a) *P*-*E* hysteresis loops of Ba(Ti_{0.9}Ce_{0.1})O₃ ceramic measured under the field of 45 kV/cm at the frequency of 10 Hz. (b) Evolution of polarization with temperature of Ba(Ti_{1-x}Ce_x)O₃ ceramics (*x* = 0.1, 0.15

and 0.2) under the field of 45 kV/cm. (c) Pyroelectric coefficient of Ba(Ti_{1-x}Ce_x)O₃ ceramics (*x* = 0.1, 0.15 and 0.2) under the field of 45 kV/cm

Table 2 Temperatures of several properties of Ba(Ti_{1-x}Ce_x)O₃ ceramics ($x = 0.10, 0.15$ and 0.20) measured at 45 kV/cm

x	$T_{\varepsilon\max}$ (K)	$(P/\varepsilon T)_{\max}$ ($\mu\text{C}/\text{cm}\cdot\text{K}$)	$T_{(P/T)\max}$ (K)	ΔT_{\max} (K)	$(\Delta T/\Delta E)_{\max}$ ($10^{-6} \text{K}\cdot\text{m}/\text{V}$)	$T_{\Delta T\max}$ (K)	ΔS_{\max} ($\text{J}/\text{kg}\cdot\text{K}$)	$(\Delta S/\Delta E)_{\max}$ ($10^{-6} \text{J}\cdot\text{m}/\text{kg}\cdot\text{K}\cdot\text{V}$)	$T_{\Delta S\max}$ (K)
0.10	378	-5.647	408	0.41	0.090	413	0.45	0.100	408
0.15	358	-3.010	393	0.21	0.046	398	0.24	0.053	393
0.20	318	-2.854	363	0.18	0.040	368	0.23	0.051	363

pyroelectric coefficient. The largest isothermal entropy change responsivity of $0.111 \times 10^{-6} \text{J}\cdot\text{m}/(\text{kg}\cdot\text{K}\cdot\text{V})$ among all magnitudes of electric field is achieved at the field of 20 kV/cm.

According to results reported by Han [21], the pure BaTiO₃ ceramics implies the largest adiabatic temperature change about 1.1 K at 30 kV/cm, which is larger than the results of Ba(Ti_{0.9}Ce_{0.1})O₃ ceramics. The temperature dependence of electrocaloric effect of the pure BaTiO₃ ceramics indicates a sharp peak in the period of 10 K, while Ba(Ti_{0.9}Ce_{0.1})O₃ ceramics maintain comparable electrocaloric effect in a broaden temperature period (>25 K). The varied tendency of electrocaloric effect can be explained by the nature of diffuse phase transition. In diffuse ferroelectrics, the PNRs can persist in a broad

temperature range around dielectric peak temperature, and the PNRs are very sensitive to frequency and magnitude of external electric field. Electrocaloric is directly related to the number of polarized states in material, the electrocaloric effect can maintain a comparable value in diffuse ferroelectrics over a broad temperature range. The temperature of maximal electrocaloric effect is the point where the number of polarized states changes most fast, it is also the temperature where the number of PNRs changes most fast.

Pyroelectric effect is the converse effect of electrocaloric effect, the quantity of pyroelectric effect can be evaluated via Olsen cycle [37, 38]. As can be seen in Fig. 8, two polarization hysteresis loops measured at high temperature and low temperature are presented. To measure the pyroelectric energy harvesting, the range of electric field (E_L and E_H) should be

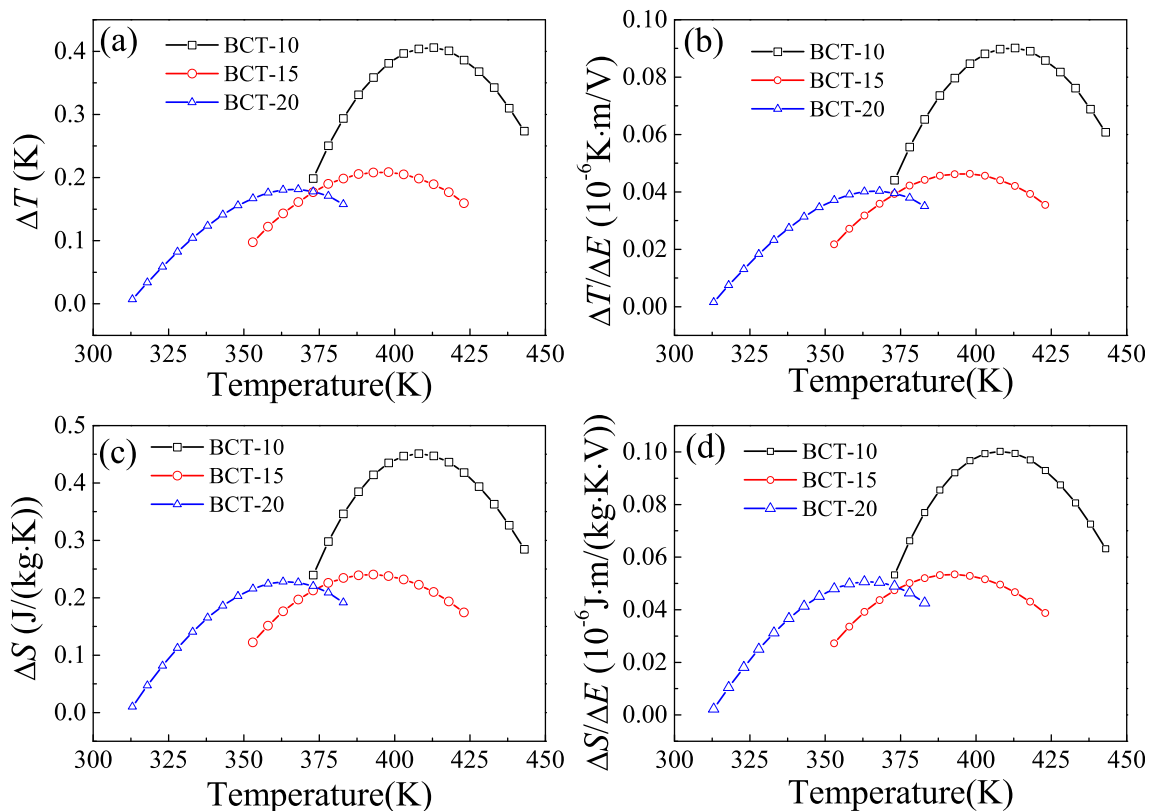


Fig. 6 Temperature dependence of (a) electrocaloric temperature change and (b) electrocaloric temperature change responsivity of Ba(Ti_{1-x}Ce_x)O₃ ceramics ($x = 0.1, 0.15$ and 0.2) under the field of 45 kV/cm. Temperature

dependence of (c) electrocaloric entropy change and (d) electrocaloric entropy change responsivity of Ba(Ti_{1-x}Ce_x)O₃ ceramics ($x = 0.1, 0.15$ and 0.2) under the field of 45 kV/cm

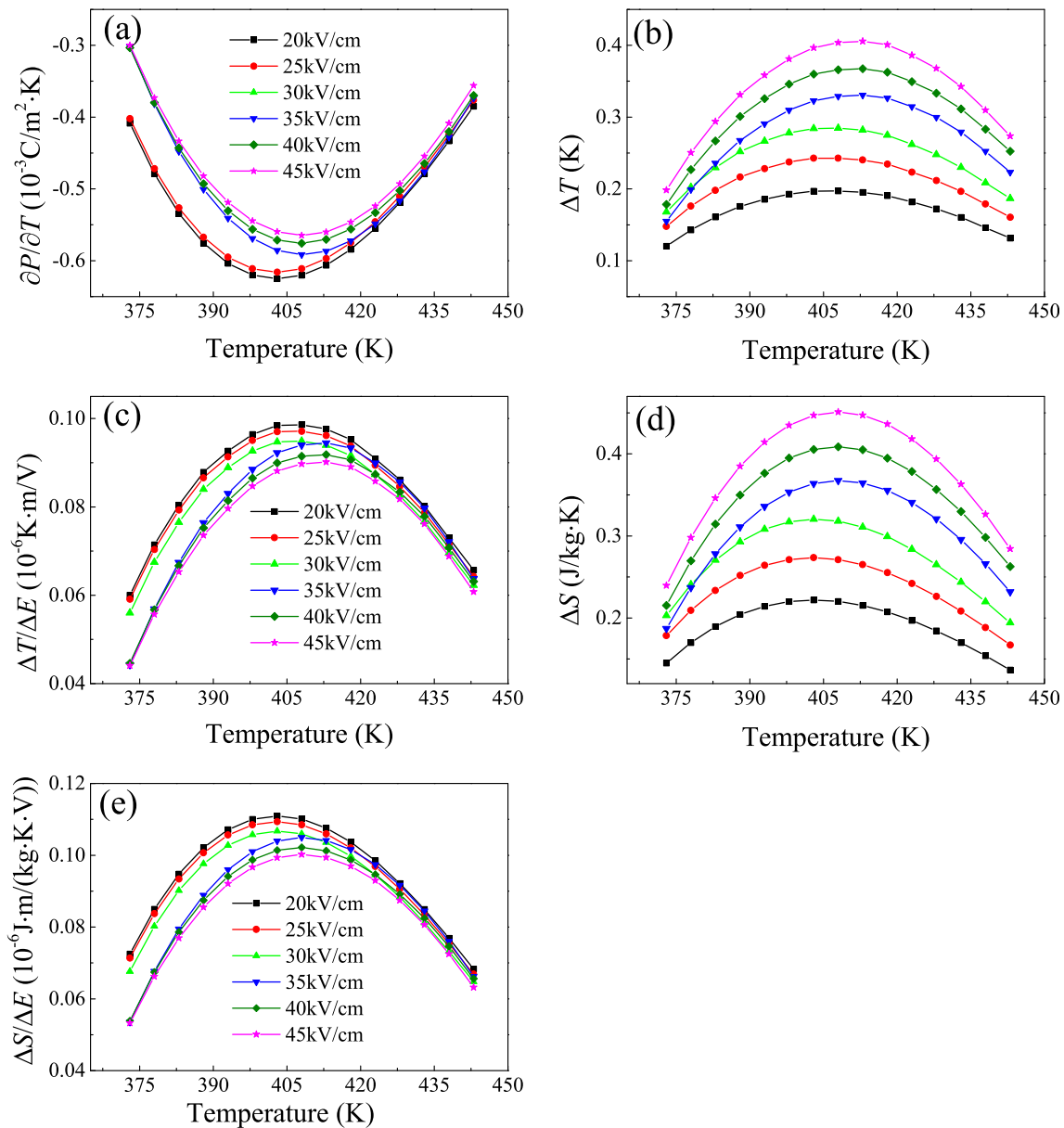


Fig. 7 Different parameters of Ba(Ti_{0.9}Ce_{0.1})O₃ ceramic measured at 20, 25, 30, 35, 40 and 45 kV/cm. Temperature dependence of (a) pyroelectric coefficient, (b) electrocaloric temperature change, (d) electrocaloric

entropy change, (c) electrocaloric temperature change responsivity and (e) electrocaloric entropy change responsivity

selected. The energy density of pyroelectric energy harvesting achieved in specialized temperature and electric field range equals the area enclosed by the green line:

$$W = \oint E dP$$

The Olsen cycle concludes two isothermal processes and two isoelectric processes, proceeding clockwise each step works for cooling. Figure 9(a)-(c) present pyroelectric energy densities of Ba(Ti_{1-x}Ce_x)O₃ ceramics, the E_L is kept 0 kV/cm, T_{LS} are 373 K, 353 K and 313 K for Ba(Ti_{1-x}Ce_x)O₃ ceramics (x = 0.1, 0.15 and 0.2). Broadening the temperature range and

electric field can improve the pyroelectric energy densities, Ba(Ti_{0.9}Ce_{0.1})O₃ ceramics show the largest pyroelectric energy density of 0.14 J/cm³ when E_H equals 45 kV/cm and T_H equals 443 K. Figure 9(d) shows the T_H dependence of pyroelectric energy densities of Ba(Ti_{1-x}Ce_x)O₃ ceramics, the E_L is kept 0 kV/cm, T_{LS} are 373 K, 353 K and 313 K for Ba(Ti_{1-x}Ce_x)O₃ ceramics (x = 0.1, 0.15 and 0.2), while E_H is kept 45 kV/cm. At specialized temperature the pyroelectric energy density increases slower as the electric field increases, for the pyroelectric coefficient at low electric field is larger than that at high electric field. There exists a temperature for each composition where the pyroelectric energy density varies fastest,

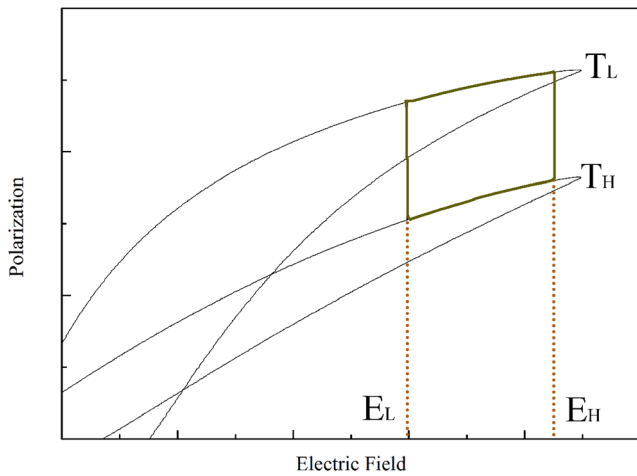


Fig. 8 Diagram of pyroelectric energy conversion mechanism using polarization hysteresis loops measured at two different temperatures based on Olsen cycle. The area enclosed by the green line represents the energy density of pyroelectric energy harvesting

i.e., 413 K, 403 K, 363 K for $\text{Ba}(\text{Ti}_{1-x}\text{Ce}_x)\text{O}_3$ ceramics ($x = 0.1, 0.15$ and 0.2). And the pyroelectric coefficient shows a peak value at these temperatures. For each composition the curve increases linearly with T_H , which is typical behavior of diffuse ferroelectrics.

4 Conclusion

The diffusivity of phase transition is strengthened by substituting Ti^{4+} by Ce^{4+} cations. The maximal pyroelectric coefficient decreases, and the extent of corresponding temperature deviating from the dielectric peak temperature to higher temperature increases with increasing the content of Ce^{4+} cations. The adiabatic temperature change and isothermal entropy change display the same tendency as that of the pyroelectric coefficient. The $\text{Ba}(\text{Ti}_{0.9}\text{Ce}_{0.1})\text{O}_3$ ceramic shows the largest adiabatic temperature change of 0.41 K and the largest isothermal entropy change of 0.45 J/(kg·K) among all compositions. Accordingly, the adiabatic temperature change responsivity is 0.090×10^{-6} K·m/V, and the isothermal entropy change responsivity is 0.10×10^{-6} J·m/(kg·K·V). For individual composition, the absolute value of pyroelectric coefficient decreases with increasing the magnitude of applied electric field, and the temperature of maximal pyroelectric coefficient deviates from the dielectric peak temperature to higher temperature. The present work sheds light into ECE of diffuse ferroelectrics, $\text{Ba}(\text{Ti}_{0.9}\text{Ce}_{0.1})\text{O}_3$ ceramics show the largest pyroelectric energy density of 0.14 J/cm³ among all compositions.

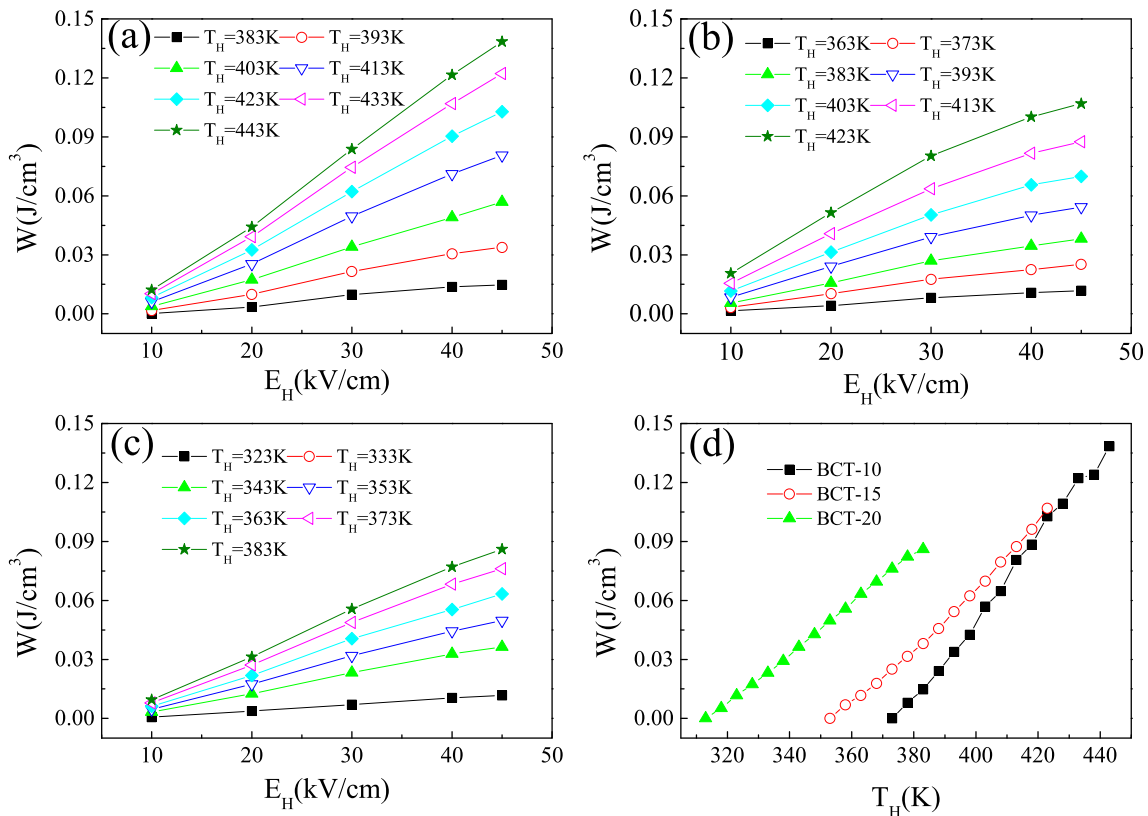


Fig. 9 E_H dependence of pyroelectric energy densities of $\text{Ba}(\text{Ti}_{1-x}\text{Ce}_x)\text{O}_3$ ceramics: (a) $x = 0.1$, (b) $x = 0.2$ and (c) $x = 0.3$ at different T_{HS} . E_L keeps 0 kV/cm, while T_{LS} are 373 K, 353 K and 313 K for $x = 0.1, 0.15$ and 0.2 , respectively. (d) T_H dependence of pyroelectric energy densities of

$\text{Ba}(\text{Ti}_{1-x}\text{Ce}_x)\text{O}_3$ ceramics ($x = 0.1, 0.15$ and 0.2). E_L keeps 0 kV/cm, E_H keeps 45 kV/cm, while T_{LS} are 373 K, 353 K and 313 K for $x = 0.1, 0.15$ and 0.2 , respectively

Acknowledgements This work was financially supported by National Natural Science Foundation of China under Grant No. 51772266, and Natural Science Foundation of Zhejiang Province under Grand No. LY15E020003.

References

- C.B. Sawyer, C.B. Tower, Rochelle salt as a dielectric. *Phys. Rec. B* **35**(3), 269–273 (1930)
- A.S. Mischenko, Q. Zhang, J.F. Scott, R.W. Whatmore, N.D. Mathur, Giant electrocaloric effect in thin film $\text{PbZr}_{0.95}\text{Ti}_{0.05}\text{O}_3$. *Science* **311**, 1270 (2006)
- M.E. Lines, A.M. Glass, *Principles and Applications of Ferroelectric and Related Materials* (Oxford University Press, New York, 1977)
- R.W. Whatmore, Pyroelectric devices and materials. *Rep. Prog. Phys.* **49**(12), 1335–1386 (1986)
- S.B. Lang, D.K. Das-Gupta, in *Handbook of Advanced Electronic and Photonic Materials and Devices*, ed. by H. S. Nalwa. Pyroelectricity: Fundamentals and Applications, vol 4 (Academic Press, San Diego, 2001), pp. 1–54
- D. Lingam, A.R. Parikh, J. Huang, A. Jain, M. MinaryJolandan, Nano/microscale pyroelectric energy harvesting: Challenges and opportunities. *Int. J. Smart Nano Mater.* **4**(4), 229–245 (2013)
- C.R. Bowen, J. Taylor, E. LeBoulbar, D. Zabeck, A. Chauhan, R. Vaish, Pyroelectric materials and devices for energy harvesting applications. *Energy Environ. Sci.* **7**(12), 3836–3856 (2014)
- N. Abdelmoula, H. Chaabane, H. Khemakem, R. von der Muhll, A. Simon, Relaxor or Classical Ferroelectric Behavior in A-Site Substituted Perovskite Type $\text{Ba}_{1-x}(\text{Sm}_{0.5}\text{Na}_{0.5})_x\text{TiO}_3$. *Solid State Sci.* **8**, 880–887 (2006)
- R. Farhi, M. El Marssi, A. Simon, J. Ravez, Relaxor-like and spectroscopic properties of niobium modified barium Titanate. *Eur. Phys. J. B.* **18**, 605–610 (1999)
- T. Maiti, R. Guo, A.S. Bhalla, Structure-property phase diagram of $\text{BaZr}_x\text{Ti}_{1-x}\text{O}_3$ system. *J. Am. Ceram. Soc.* **91**(6), 1769–1780 (2008)
- X.S. Qian, H.J. Ye, Y.T. Zhang, H. Gu, X. Li, C.A. Randall, Q.M. Zhang, Giant Electrocaloric response over a broad temperature range in modified BaTiO_3 ceramics. *Adv. Funct. Mater.* **24**(9), 1300–1305 (2014)
- Z.K. Liu, X. Li, Q.M. Zhang, Maximizing the number of coexisting phases near invariant critical points for giant electrocaloric and electromechanical responses in ferroelectrics. *Appl. Phys. Lett.* **101**, 954–959 (2012)
- Y. Bai, H. Xi, L.J. Qiao, Effect of donor doping in B sites on the electrocaloric effect of $\text{BaTi}_{1-x}\text{Nb}_x\text{O}_3$ ceramics. *RSC Adv.* **5**(88), 71873–71877 (2015)
- Z. Luo, D. Zhang, Y. Liu, D. Zhou, Y. Yao, C. Liu, B. Dkhil, X. Ren, X. Lou, Enhanced electrocaloric effect in lead-free $\text{BaTi}_{1-x}\text{Sn}_x\text{O}_3$ ceramics near room temperature. *Appl. Phys. Lett.* **105**, 102904 (2014)
- H. Kaddoussi, Y. Gagou, A. Lahmar, J. Belhadi, B. Allouche, J.-L. Dellis, M. Courty, H. Khemakem, M. El Marssi, Room temperature electro-caloric effect in lead-free $\text{Ba}(\text{Zr}_{0.1}\text{Ti}_{0.9})_{1-x}\text{Sn}_x\text{O}_3$ ($x=0, x=0.075$) ceramics. *Solid State Commun.* **201**, 64–67 (2015)
- X. Zhang, L. Wu, S. Gao, J.Q. Liu, B. Xu, Y.D. Xia, J. Yin, Z.G. Liu, Large electrocaloric effect in $\text{Ba}(\text{Ti}_{1-x}\text{Sn}_x)\text{O}_3$ ceramics over a broad temperature region. *AIP Adv.* **5**(4), 047134 (2015)
- Y. Zhou, Q. Lin, W. Liu, D. Wang, Compositional dependence of electrocaloric effect in lead-free $(1-x)\text{Ba}(\text{Zr}_{0.2}\text{Ti}_{0.8})\text{O}_3-x(\text{Ba}_{0.7}\text{Ca}_{0.3})\text{TiO}_3$ ceramics. *RSC Adv.* **6**, 14084 (2016)
- H. Kaddoussi, Y. Gagou, A. Lahmar, B. Asbani, B. Allouche, J.-L. Dellis, G. Cordoyiannis, H. Khemakem, M. El Marssi, Indirect and direct electrocaloric measurements of $(\text{Ba}_{1-x}\text{Ca}_x)(\text{Zr}_{0.1}\text{Ti}_{0.9})\text{O}_3$ ceramics ($x=0.05, 0.20$). *J. Alloys Compd.* **667**, 198–203 (2016)
- B. Asbani, J.-L. Dellis, A. Lahmar, M. Courty, M. El Amjoud, Y. Gagou, K. Djellab, D. Mezzane, Z. Kutnjak, M. El Marssi, Lead-free $\text{Ba}_{0.8}\text{Ca}_{0.2}(\text{Zr}_x\text{Ti}_{1-x})\text{O}_3$ ceramics with large electrocaloric effect. *Appl. Phys. Lett.* **106**, 042902 (2015)
- S. Xie, Y. Bai, F. Han, S. Qin, J. Li, L. Qiao, D. Guo, Distinct effects of Ce doping in a or B sites on the electrocaloric effect of BaTiO_3 ceramics. *J. Alloys Compd.* **724**, 163–168 (2017)
- F. Han, Y. Bai, L.J. Qiao, D. Guo, A systematic modification of the large electrocaloric effect within a broad temperature range in rare-earth doped BaTiO_3 ceramics. *J. Mater. Chem. C* **4**(9), 1842–1849 (2016)
- X. Moya, E. Stern-Taulats, S. Crossley, D. González-Alonso, S. Kar-Narayan, A. Planes, L. Mañosa, N.D. Mathur, Giant Electrocaloric strength in single-crystal BaTiO_3 . *Adv. Mater.* **25**(9), 1360–1365 (2013)
- B. Rožic, M. Kosec, H. Uršic, J. Holc, B. Malic, Q.M. Zhang, R. Blinc, R. Pirc, Z. Kutnjak, Influence of the critical point on the electrocaloric response of relaxor ferroelectrics. *J. Appl. Phys.* **110**(6), 064118 (2011)
- Y. Bai, K. Ding, G.P. Zheng, S.Q. Shi, L. Qiao, Entropy-change measurement of electrocaloric effect of BaTiO_3 single crystal. *Phys. Status Solidi A* **209**(5), 941–944 (2012)
- Y. Bai, X. Han, K. Ding, L.J. Qiao, Combined effects of diffuse phase transition and microstructure on the electrocaloric effect in $\text{Ba}_{1-x}\text{Sr}_x\text{TiO}_3$ ceramics. *Appl. Phys. Lett.* **103**, 162902 (2013)
- G.C. Lin, X.M. Xiong, J.X. Zhang, Q. Wei, Latent heat study of phase transition in $\text{Ba}_{0.73}\text{Sr}_{0.27}\text{TiO}_3$ induced by electric field. *Therm. Anal. Calorim.* **81**, 41–44 (2005)
- M. Sanlialp, V.V. Shvartsman, M. Acosta, B. Dkhil, D.C. Lupascu, Strong electrocaloric effect in lead-free $0.65\text{Ba}(\text{Zr}_{0.2}\text{Ti}_{0.8})\text{O}_3-0.35(\text{Ba}_{0.7}\text{Ca}_{0.3})\text{TiO}_3$ ceramics obtained by direct measurements. *Appl. Phys. Lett.* **106**, 062901 (2015)
- K.S. Srikanth, R. Vaish, Enhanced electrocaloric, pyroelectric and energy storage performance of $\text{BaCe}_x\text{Ti}_{1-x}\text{O}_3$ ceramics. *J. Eur. Ceram. Soc.* **37**(13), 3927–3933 (2017)
- S.M. Zeng, X.G. Tang, Q.X. Liu, Y.P. Jiang, M.D. Li, W.H. Li, Z.H. Tang, Electrocaloric effect and pyroelectric properties in Ce-doped $\text{BaCe}_x\text{Ti}_{1-x}\text{O}_3$ ceramics. *J. Alloys Compd.* **776**, 731–739 (2019)
- J. Rodriguez-Carvajal, Recent advances in magnetic structure determination by neutron powder diffraction. *Physica B* **192**(1-2), 55–69 (1993)
- G. Burns, F.H. Dacol, Glassy polarization behavior in ferroelectric compounds $\text{Pb}(\text{Mg}_{1/3}\text{Nb}_{2/3})\text{O}_3$ and $\text{Pb}(\text{Zn}_{1/3}\text{Nb}_{2/3})\text{O}_3$. *Solid State Commun.* **48**(10), 853–856 (1983)
- S.B. Vakhrushev, B.E. Kvyatkovy, A.A. Nabereznov, N.M. Okuneva, B.P. Toperverg, Glassy phenomena in disordered perovskite-like crystals. *Ferroelectrics* **90**(1), 173–176 (1989)
- K. Hirota, Z.G. Ye, S. Wakimoto, P.M. Gehring, G. Shirane, Neutron diffuse scattering from polar nanoregions in the relaxor $\text{Pb}(\text{Mg}_{1/3}\text{Nb}_{2/3})\text{O}_3$. *Phys. Rev. B* **65**(10), 104105 (2002)
- V.V. Shvartsman, W. Kleemann, J. Dec, Z.K. Xu, S.G. Lu, Diffuse phase transition in $\text{BaTi}_{1-x}\text{Sn}_x\text{O}_3$ ceramics: An intermediate state between ferroelectric and relaxor behavior. *J. Appl. Phys.* **99**(12), 124111 (2006)

35. V.P. Bovtoun, M.A. Leshchenko, Two dielectric contributions due to domain/cluster structure in the ferroelectrics with diffused phase transitions. *Ferroelectrics* **190**(1), 185–190 (1997)
36. A. Chen, Y. Zhi, DC electric-field dependence of the dielectric constant in polar dielectrics: Multipolarization mechanism model. *Phys. Rev. B* **69**, 174109 (2004)
37. A. Navid, L. Pilon, Pyroelectric energy harvesting using Olsen cycles in purified and porous poly(vinylidene fluoride-trifluoroethylene) [P(VDF-TrFE)] thin films. *Smart Mater. Struct.* **20**, 025012 (2011)
38. I.M. McKinley, L. Pilon, Phase transitions and thermal expansion in pyroelectric energy conversion. *Appl. Phys. Lett.* **102**(2), 023906 (2013)

Publisher's note Springer Nature remains neutral with regard to jurisdictional claims in published maps and institutional affiliations.